# Constructing pseudo-orbits on invariant manifolds of maps as seeds for boundary value problems

Dana C'Julio, Sanaz Amani, Sam Doak, Bernd Krauskopf and Hinke M. Osinga
Department of Mathematics, The University of Auckland
Private Bag 92019, Auckland 1142, New Zealand

22 January 2026

**Abstract**

An important tool for understanding complicated dynamics in the iteration of a map is the ability to find certain orbits of interest. In particular, connecting orbits between saddle fixed points and/or saddle periodic points are special orbits that are closely associated with intersections of stable or unstable manifolds. They can be found numerically and then be continued in parameters as solutions of suitably formulated boundary value problems (BVPs). We address the key issue that one needs to find a seed solution when solving a BVP with Newton's method. In our setting, a seed solution takes the form of a finite sequence of points that almost satisfies the required conditions of the BVP. To construct such seeds, we modify a numerical method that finds and represents a one-dimensional stable or unstable manifold of a diffeomorphism in such a way that a so-called pseudo-orbit for any computed point is readily available from the data. We explain how pseudo-orbits of relevant points on a computed invariant manifold can successfully be used as seeds for solving a variety of BVPs in a systematic and efficient way. We illustrate our findings with two three-dimensional diffeomorphism with complicated dynamics, by computing many orbits on an invariant manifold that end in a chosen section, as well as numerous homoclinic and heteroclinic connectiong orbits.

## 1 Introduction

Many interesting dynamical systems are given in the form of a map that evolves points in phase space in discrete time by iteration. Such maps can be given explicitly, as is the case for the Hénon map [8], or they can be defined by a vector field as a Poincaré map to a specified section [13]. Both of these and many other examples are diffeomorphisms, that is, smooth maps with smooth inverses, and we restrict our attention to this class of dynamical systems, for which every point in phase space has a unique forward and a unique backward trajectory.

Describing and classifying the possibly very intricate dynamics produced by a diffeomorphism is a difficult task. The key is to find the relevant invariant sets: the fixed points and periodic orbits, as well as their stable and unstable manifolds when they are saddles. For example, a transverse intersection between the stable and unstable manifolds of the same fixed or periodic point gives rise to a hyperbolic set with chaotic Smale horseshoe dynamics [24]. Furthermore, non-transverse intersections of manifolds, such as homoclinic tangencies and heterodimensional cycles, are the primary mechanism for generating robust nonhyperbolic dynamics [2, 7, 20].

Stable and unstable manifolds cannot generally be found analytically and must, instead, be computed numerically. Algorithms for computing one-dimensional manifolds of fixed points have been available for a while, and most use the iteration of an initial (approximate) fundamental domain sufficiently near the fixed point; see, for example, [12, 26]. One-dimensional manifolds can also be computed step-by-step as an arclength parametrised curve by adding one point at a time until a sufficient arclength has been reached [18]. Stable and unstable manifolds of periodic points are usually found in the same way by considering a suitable iterate of the map. Crucially, the quality of the computed one-dimensional manifold is controlled by ensuring that mesh points lie closer to each other when the curvature of the manifold is large [12, 18]. We remark that already the numerical computation of stable and unstable manifolds of dimension two is a much more difficult task, as it requires the construction of a two-dimensional mesh; see [17]. Therefore, in higher dimensions, computational efforts tend to be focussed on special orbits on such manifolds only, such as orbits that end in a section of interest, or homoclinic and heteroclinic orbits. An immediate and natural problem formulation is in the form of a boundary value problem (BVP) with conditions that ensure the solution is an orbit of the underlying dynamical system, and boundary conditions that characterise the special nature of the solution of interest.

The work presented here is based on the algorithm described in [5], which uses fundamental domain iteration with subsequent (vectorised) mesh refinement motivated by [18]. The computed one-dimensional manifold is represented as an arclength-parametrised curve, specifically, as a list of mesh points that are ordered by arclength distance from the saddle fixed point. We show here how this algorithm can be modified with minimal additional computational effort and data storage requirements, so that a finite pseudo-orbit from or to a very small neighbourhood of the fixed point is readily available for each mesh point of the computed one-dimensional manifold. Pseudo-orbits are a concept associated with *shadowing*, which guarantees the existence of a nearby actual (finite) orbit of the diffeomorphism; see [4, 14, 25, 27] and references therein. Hence, pseudo-orbits are natural seeds for finding an initial solution of a BVP with Newton's method. As soon as a first solution has been found, it can subsequently be continued in system parameters as part of a bifurcation study of associated global objects, and additional seeds to compute an entire solution family are automatically constructed by the continuation algorithm; see [15, 16] for background information. In other words, our method provides the key step of constructing the seed for the very first solution to a BVP, and offers a systematic approach to identifying and computing entire solution families that represent important global objects in a dynamical system given by a diffeomorphism. As we will show with two examples, this capability is especially useful for the case study of diffeomorphisms with complicated geometric structures associated with robust non-hyperbolic dynamics. In particular, these systems may exhibit: blenders, which are hyperbolic sets with invariant manifolds that act as if they were of higher dimension; and heterodimensional cycles between periodic points with unstable manifolds of different dimensions.

This paper is organised as follows. In Section 2 we introduce some notation and then describe how we compute a one-dimensional invariant manifold including all its pseudo-orbits; the MATLAB implementation of our algorithm can be downloaded from `github.com/dcjulio`. In Section 3, we consider a family of three-dimensional Hénon-like diffeomorphisms and show how to find orbits on the one-dimensional unstable manifold of a fixed point that end in a chosen two-dimensional section. A large number of such orbits—and, hence, the

intersection set of the manifold with the section—can then be continued to show when and how a blender arises as a relevant parameter of the Hénon-like family is changed. In Section 4, we demonstrate how to use pseudo-orbits to find connecting orbits in a three-dimensional diffeomorphism with a complicated nonwandering set and heterodimensional cycles. Specifically, we find many different structurally stable homoclinic orbits to one and the same saddle fixed point, as well as many non-transverse connecting orbits between two fixed points of different index (number of unstable eigenvalues). Section 5 presents a conclusion and discussion of directions for future work.

## 2 Computing a one-dimensional invariant manifold with its pseudo-orbits

We consider a diffeomorphism

$$f : \mathbb{R}^n \to \mathbb{R}^n$$

with a saddle fixed point $p = f(p) \in \mathbb{R}^n$ that has a single positive, real, unstable eigenvalue $\lambda_u > 1$. Our goal is to compute its unstable manifold

$$W^u(p) = \{x \in \mathbb{R}^n \mid f^{-k}(x) \to p \text{ as } k \to \infty\},$$

which is a one-dimensional smooth curve that is tangent at $p$ to the unstable eigenspace spanned by an eigenvector $\mathbf{v}_u$ of $\lambda_u$ [23]. Note that $W^u(p)$ consists of infinitely many orbits that converge to $p$ under iteration of the inverse $f^{-1}$. We assume $\lambda_u > 1$, which means that $W^u(p)$ is orientation preserving; to find $W^u(p)$ for the orientation-reversing case with negative $\lambda_u$ one considers the second iterate $f^2$. Likewise, one-dimensional unstable manifolds of periodic points can be computed by considering the corresponding higher iterate of $f$. Finally, in our setting, any one-dimensional stable manifold can, by definition, be computed as the unstable manifold of $f^{-1}$.

Since $W^u(p)$ is orientation preserving, it consists of two $f$-invariant branches (on either side of $p$). Each branch is computed separately, up to a finite arclength, and represented as a list $M$ of suitably spaced mesh points that are ordered according to their (approximate) arclength along $W^u(p)$ from $p$. We are interested in computing $W^u(p)$ in such a way that the resulting data allows us to construct a pseudo-orbit [27] for any computed point in the mesh $M$.

In our setting, a pseudo-orbit is a finite sequence $\{\widetilde{a}_{-N}, \ldots, \widetilde{a}_0\}$ of length $N+1$ such that the image of the point $\widetilde{a}_j$, for $j = 1, \ldots, N$, lies in an $\varepsilon$-ball centred at the next point in the sequence for some $\varepsilon > 0$; here, $\varepsilon$ is expected to be small, so that we can think of the sequence as an approximate finite orbit of $f$. We say that $\{\widetilde{a}_j\}_{-N \le j \le 0}$ is a pseudo-orbit, or more precisely, an $\varepsilon$-pseudo-orbit of a point on $W^u(p)$ if the following conditions are satisfied

$$\begin{cases} \widetilde{a}_0 \in M, \\ \forall j \in \{1, \ldots, N\} \ \|f(\widetilde{a}_{-j}) - \widetilde{a}_{-(j-1)}\| < \varepsilon, \text{ and} \\ \|\widetilde{a}_{-N} - p\| < \varepsilon. \end{cases} \tag{1}$$

In our notation, we use a negative sign for the subscripts of the points $\widetilde{a}_j$ to indicate that we assume $\widetilde{a}_0$ lies approximately on $W^u(p)$ and its pseudo-orbit $\{\widetilde{a}_j\}_{-N \le j \le 0}$ approximates

a true (finite) orbit on $W^u(p)$; a sequence with positive subscripts suggests a pseudo-orbit for $f$ approximating a true orbit on $W^s(p)$, which we will encounter in Section 4.

Note that there always exists $\varepsilon > 0$ so that any $\{\widetilde{a}_j\}_{-N \le j \le 0}$ with $\widetilde{a}_0 \in M$ is a pseudo-orbit of a point on $W^u(p)$. We take advantage of this fact and construct sequences $\{\widetilde{a}_j\}_{-N \le j \le 0} \subseteq M$, that is, each of the points $\widetilde{a}_j$ in the pseudo-orbit is a mesh point of the computed manifold $W^u(p)$. Consequently, our construction is such that $\varepsilon$ depends on the *mesh size* $\Delta_{\max}$ of $M$: as $\Delta_{\max}$ decreases, so does the minimum value for $\varepsilon$, which guarantees that the $\varepsilon$-pseudo-orbit will converge to a true (finite) orbit on $W^u(p)$ in the limit $\Delta_{\max} \to 0$. Hence, provided we approximate $W^u(p)$ with a sufficiently fine mesh $M$, appropriate pseudo-orbits can be used as seeds for Newton's method to find orbits on $W^u(p)$ up to any precision as solutions of a suitable boundary value problem (BVP).

### 2.1 Generating a mesh representation of the manifold

For completeness, we briefly explain our algorithm from [5] that computes a mesh $M$ resprresenting one branch of $W^u(p)$ up to a finite arclength $L$; the algorithm constructs $M$ in an iterative manner as a sequence of images under $f$ of a *fundamental domain* of $W^u(p)$. A fundamental domain has the defining property that it is intersected exactly once by every orbit of $f$ on $W^u(p)$. Hence, we start by constructing a mesh $M_0$ of a fundamental domain near $p$, and proceed by adding additional mesh representations of successive images of this fundamental domain until the required arclength is reached (or exceeded). The total number of images needed, denoted $K$, depends on $L$ and the choice of the first fundamental domain; in what follows, we merely assume that $K$ is sufficiently large.

To define $M_0$, we take a set $\{s_1, \ldots, s_m\}$ of equally spaced and ordered points in the unstable eigenspace from $p$ up to $s_m = p + \delta\, \mathbf{v}_u$, with $0 < \delta \ll 1$. We then define

$$M_0 = \{s_m, f(s_{j^*}), \ldots, f(s_m)\},$$

where $s_{j^*}$ is the first point in the sequence that satisfies $\|f(s_{j^*}) - p\| > \delta$. If $\delta$ is sufficiently small, the linear dynamics dominates and $\|f(s_{j^*}) - p\| \approx \lambda_u \|s_{j^*} - p\| = \lambda_u \frac{j^*}{m} \delta$. Hence, $f(s_{j^*})$ is expect to map 'beyond' $s_m$ as soon as $j^* > m/\lambda_u$. To ensure that $\delta$ is chosen sufficiently small, we check that the distance $\eta$ from the endpoint $s_m$ to the line segment between $p$ and $f(s_{j^*})$ is of order $O(\delta^2)$.

By construction, all points in $M_0$ lie in a very small neighbourhood of $p$. We define each of their pseudo-orbits as the mesh points themselves with $N = 0$; it is straightforward to verify that all conditions (1) are satisfied for $\varepsilon \approx \lambda_u\, \delta$.

The construction of $M_0$ is illustrated in Fig. 1 for $m = 5$ and $\delta = 10^{-7}$. Shown is actual data for the (first two components of the) Hénon-like family $H$, defined in Section 3, with fixed point $p = p^+$; see already (3) with parameters given by (4). We consider $f = H^2$ because the unstable eigenvalue $\lambda^u \approx -3.5428$ of $p = p^+$ is negative. For Fig. 1, we applied a translation and a rotation of the $(x, y)$-plane, such that $p$ lies at the origin and its unstable eigenvector $\mathbf{v}_u$ is horizontal. Observe that $j^* = 1$ in Fig. 1; indeed, the unstable eigenvalue associated with $H^2$ is $(\lambda_u)^2$, so that $j^* = \lceil 5/(-3.5428)^2 \rceil$. The inset shows how we check that $\delta$ is sufficiently small: the point $s_5$ lies at distance $\eta = 1.23 \times 10^{-14} = O(\delta^2)$ from the line through $p$ and $f(s_1)$.

The mesh $M_0$, preceeded by the fixed point $p$, represents the first computed segment of $W^u(p)$. We obtain longer segments by generating mesh representations $M_k$, for $1 \le k \le K$,

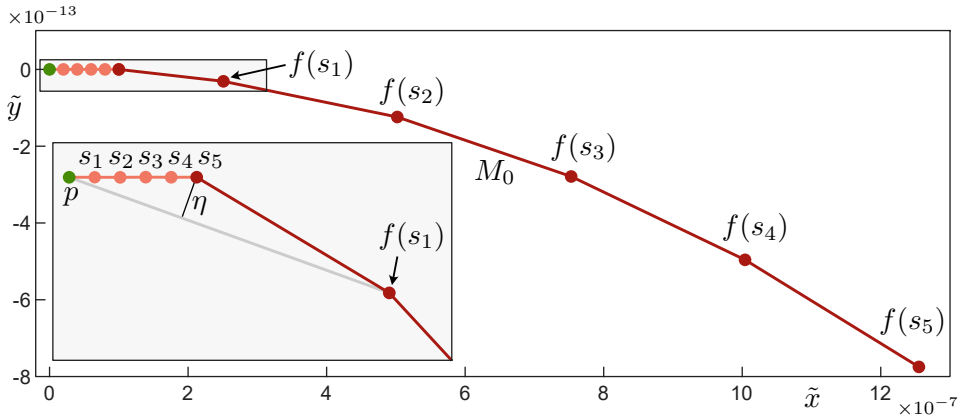


Figure 1: Construction of $M_0$ (dark red) representing a fundamental domain on $W^u(p)$ for the map $H$, defined in (3) with (4); here, $\tilde{x}$ and $\tilde{y}$ are the first two components of $H$ after translation and rotation so that $p = p^+$ lies at the origin and $\mathbf{v}_u$ is horizontal. Shown are the fixed point $p$ (green dot) and $m = 5$ points $\{s_1, \ldots, s_5\}$ (orange dots) on the unstable eigenspace (orange line), together with their images. The inset shows an enlargement near $p$ to illustrate the line segment (grey) between $p$ and $f(s_1)$ and its distance $\eta$ to $s_5$; note the large difference in scale between $\tilde{x}$ and $\tilde{y}$.

of the next $K$ fundamental domains as images under $f$. More precisely, at step $k$, we form the set $M_k^{(0)} := f(M_{k-1}) = \{f(q_{m_{k-1}}), \ldots, f(q_{m_k})\}$ and then add (or remove) mesh points in stages until the set $M_k := M_k^{(i_k)}$ at stage $i_k$ satisfies curvature-dependent accuracy conditions, which are a combination of those introduced in [12, 18]. Specifically, we define the distance $\Delta_j$ between consecutive mesh points $q_j$ and $q_{j+1}$ in $M_k^{(i_k)}$, and the angle $\alpha_j$ between consecutive triplets of points centered at $q_j$, and verify the following requirements in this order:

(A) $\Delta_j < \Delta_{\max}$, to guarantee a suitable baseline distance between mesh points;

(B) $\alpha_j < \alpha_{\max}$, to ensure an overall bound on the angle;

(C) $\Delta_j\, \alpha_j < (\Delta\alpha)_{\max}$ and $\Delta_{j-1}\, \alpha_j < (\Delta\alpha)_{\max}$, to control the distance between mesh points according to the local curvature at $q_j$; and

(D) $\Delta_{\min} < \Delta_j$, to ensure a suitable minimum distance between mesh points, which prevents excessive addition of new mesh points, for example, during sharp turns of the manifold.

Starting with condition (A), we check that it is satisfied for all mesh points in $M_k^{(0)}$; this is implemented in a vectorised way. If (A) is not satisfied, points are added to the mesh, the stage $i_k$ is increased, and condition (A) is checked again. The process is repeated until condition (A) is satisfied for all points in $M_k^{(i_k)}$; only then is the next condition considered, in the same way, and so on, until $M_k := M_k^{(i_k)}$ satisfies (A)–(D) and the step is complete.

Crucially, every point that is added to $M_k$ is found as the image of a point on the previous fundamental domain, as represented by piecewise-cubic Hermite interpolation between mesh

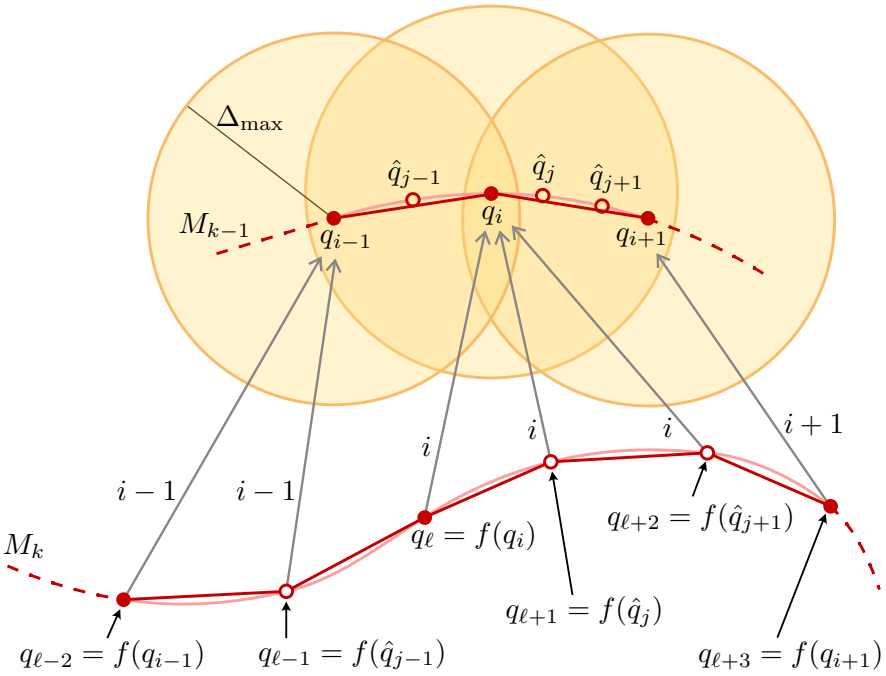


Figure 2: Illustration of the integer pointers (grey arrows) to previous mesh points in $M_{k-1}$ that are approximate preimages of mesh points in $M_k$. The mesh points $q_{\ell-2}, \ldots, q_{\ell+3} \in M_k$ all have either $q_{i-1}, q_i, q_{i+1} \in M_{k-1}$ as preimages (red dots), or they have been added during a stage and their preimages (red open dots) lie on the cubic interpolation (light red curve) of $M_{k-1}$ in between these three points. Also shown are disks of radius $\Delta_{\max}$ (yellow) to indicate the corresponding pseudo-orbits.

points in $M_{k-1}$. This way of constructing the overall mesh $M = \cup_{0 \le k \le K} M_k$ in steps and stages ensures that $M$ represents the computed part of the branch of $W^u(p)$ to an accuracy that is controlled by $\Delta_{\max}$, $\alpha_{\max}$, $(\Delta\alpha)_{\max}$, and $\Delta_{\min}$; see [5] for more information on the mesh refinement, accuracy conditions and error control.

## 2.2 Construction of pseudo-orbits of the manifold

Our approach for adding points $M_k^{(0)} = f(M_{k-1})$ in successive stages, provides us with an efficient way to record additional information that encodes pseudo-orbits of all mesh point in $M_k$ for $k \ge 1$. Since every point in $M_k$ is found either as the image of a mesh point in $M_{k-1}$ (at the first stage), or as the image of a point on the cubic interpolation through mesh points of $M_{k-1}$ (at successive stages), the preimages of the points in $M_k$ are known when they are added. We construct their pseudo-orbits by recording not their actual preimages, but merely the indices of the mesh points in $M_{k-1}$ that are closest to them. To this end, we only need to expand the data structure by equipping every mesh point $q_{\ell_j} \in M_k$ with a pointer to the respective mesh point in $M_{k-1}$; specifically, we consider the pair $(q_{\ell_j}, \ell_{j+1})$, where $\ell_{j+1}$ is the index of the point $q_{\ell_{j+1}} \in M_{k-1}$ closest to the preimage. When the preimage of $q_{\ell_j}$ is not already a mesh point, we define $q_{\ell_{j+1}} \in M_{k-1}$ as the earlier (in arclength) of the two mesh points that bound the small cubic curve segment containing the preimage;

choosing the earlier rather than closest mesh point allows for easier implementation without compromising in accuracy. This methodology is illustrated in Fig. 2 for three mesh points $q_{i-1}, q_i, q_{i+1} \in M_{k-1}$ and their images $f(q_{i-1}), f(q_i), f(q_{i+1}) \in M_k$.

Our method comprises a computationally inexpensive way of determining $\ell_{j+1}$ in a unique way. This tracking of approximate inverse images of mesh points in $M_k$ ensures that the backward image error is bounded by the distance between mesh points in $M_{k-1}$, which is at most $\Delta_{\max}$ according to accuracy condition (A). This is true for any $k$ and, therefore, for all points of the final computed mesh $M$. Hence, for any mesh point $\widetilde{a}_0 = q_{\ell_0} \in M$, the recursive expanded sequence of data points

$$\{(q_{\ell_K}, 0), (q_{\ell_{K-1}}, \ell_K), \ldots, (q_{\ell_1}, \ell_2), (q_{\ell_0}, \ell_1)\},$$

with $q_{\ell_K} \in M_0$ (and pointer index 0 to $p$), allows us to define the corresponding pseudo-orbit

$$\{q_{\ell_K}, q_{\ell_{K-1}}, \ldots, q_{\ell_1}, q_{\ell_0}\}. \tag{2}$$

By construction, $\|q_{\ell_{j+1}} - f^{-1}(q_{\ell_j})\| < \Delta_{\max}$ for the pre-specified accuracy parameter $\Delta_{\max}$. Since $f$ is a diffeomorphism, and we only consider $W^u(p)$ up to a finite arclength, i.e., $K$ is finite, the forward difference $\|f(q_{\ell_{j+1}}) - q_{\ell_j}\| < \varepsilon$ is also bounded for some $\varepsilon > 0$. While this bound is not readily computable, because it depends on local contraction rates given by Lipschitz constants, we still have that all conditions (1) are satisfied, because $q_{\ell_0} \in M$ and $\|q_{\ell_K} - p\| < \delta < \varepsilon$.

In conclusion, the sequence (2) can serve as a pseudo-orbit for either $f$ or $f^{-1}$ or both, depending on what is required for the BVP that is to be solved with this data as a seed. The fact that $\varepsilon$ is not explicitly known is not a limitation from a practical perspective: because $\varepsilon$ goes to zero linearly with $\Delta_{\max}$, it can always be guaranteed that (2) is a suitable seed also under forward iteration of $f$. As the examples in the next two sections show, we found that, when $W^u(p)$ is computed to good accuracy as a curve, the pseudo-orbits of any of the mesh points involved are successful seeds for the different BVPs. More specifically, Newton's method converges to an initial solution without a problem, regardless of whether the set-up concerns orbits of $f$ and/or $f^{-1}$.

# 3 Finding and continuing the intersection set of a one-dimensional manifold with a section

The Hénon-like family

$$H(x, y, z) = \big(y,\, \alpha - y^2 - \beta x,\, \xi z + y\big) \tag{3}$$

has been introduced and studied as the first example of an explicitly given family of diffeomorphisms that has a *blender* [5, 10, 11]. A blender is a hyperbolic set $\Lambda$ with a one-dimensional stable or unstable manifold that cannot be avoided by an open set of curves [2]. Colloquially speaking, this one-dimensional invariant manifold of $\Lambda$ acts like a surface so that one cannot 'see through it' when viewed from an open set of directions.

In [10, 11], it was shown that $H$ has a blender when the parameters $\alpha$ and $\beta$ are chosen such that the underlying Hénon map in the $(x, y)$-plane has a full Smale horseshoe, and the contraction rate $\xi$ in the $z$-direction is sufficiently close to 1. The key to numerically verifying whether $H$ has a blender lies in checking the so-called carpet property of whether

the relevant one-dimensional invariant manifold of a saddle fixed point is dense in a suitable projection. This is achieved by computing a large intersection set of the manifold with a chosen two-dimensional section $\Sigma$, taken to be a plane. These intersection points are then projected onto an interval to check for denseness; see [5, 10, 11] for details. In these references, each intersection point is computed by interpolation between mesh points on the computed one-dimensional manifold that lie either side of the chosen plane.

In a departure from this approach, we now show how to use pseudo-orbits on the invariant manifold as seeds for a BVP that defines an orbit from (very near) a saddle point to the chosen section $\Sigma$. Crucially, each final point lies exactly in $\Sigma$, and the entire orbit with this property can then be continued in any of the parameters of $H$.

To be specific, we consider the parameter choice

$$\alpha = 4.2, \quad \text{and} \quad \beta = -0.3, \tag{4}$$

for which the underlying Hénon map is known to have a full horseshoe [6]; moreover, we consider $|\xi| < 1$ sufficiently close to 1 and initially take $\xi = 0.8$. The map $H$ has two fixed points

$$p^{\pm} := \left(\rho^{\pm},\, \rho^{\pm},\, \frac{\rho^{\pm}}{1-\xi}\right), \tag{5}$$

where $\rho^{\pm} = \frac{1}{2}\left(-1-\beta \pm \sqrt{4\alpha + (1+\beta)^2}\right)$, which (certainly) exist for all $\alpha \geq 0$. For $\alpha = 4.2$, $\beta = -0.3$, and any $|\xi| < 1$, both fixed points $p^{\pm}$ have one-dimensional unstable manifolds $W^u(p^{\pm})$ and two-dimensional stable manifolds $W^s(p^{\pm})$.

We compute the intersection set of $W^u(p^+)$ with the half-plane

$$\Sigma = \{(x, y, z) \in \mathbb{R}^3 \mid x = y,\ x > 0\},$$

which contains $p^+$. While weaving through $\Sigma$, the manifold $W^u(p^+)$ makes longer and longer excursions near infinity. Therefore, we follow [5] and compactify $(x, y, z)$-space by the transformation

$$\mathcal{T}(x, y, z) = (\bar{x}, \bar{y}, \bar{z}) := \left(\frac{(x, y)}{1 + \sqrt{1 + (x^2 + y^2)}},\ \frac{z}{1 + \sqrt{1 + z^2}}\right)$$

to the cylinder

$$\mathcal{C} = \mathcal{D} \times \mathcal{I} = \{(\bar{x},\, \bar{y},\, \bar{z}) \in \mathbb{R}^3 \mid \|(\bar{x},\, \bar{y})\| \leq 1 \text{ and } |\bar{z}| \leq 1\}.$$

Its boundary $\partial\mathcal{C}$ represents infinity of $(x, y, z)$-space, and $H$ acts on the interior of $\mathcal{C}$ as the conjugate $\mathcal{T} \circ H \circ \mathcal{T}^{-1}$. For simplicity, we refer to this conjugate map as $H$ as well, and also use the same labels for its fixed points and invariant manifolds. Crucially, excursions of $W^u(p^+)$ near infinity are bounded in arclength in $\mathcal{C}$; this important property of the compactification makes it possible to find hundreds of its intersection points with $\Sigma$.

### 3.1 BVP formulation of orbits on $W^u(p^+)$ up to $\Sigma$

For the parameter values in (4), the fixed point $p^+$ has the single unstable eigenvalue $\lambda_u \approx -3.5428 < -1$ with unit eigenvector

$$\mathbf{v}_u \approx \begin{bmatrix} 0.5452 \\ -0.8383 \\ 0.0107 \end{bmatrix}.$$

Since $\lambda_u < 0$, the map $H$ is orientation reversing on $W^u(p^+)$ and we need to consider the second iterate $H^2$. To be specific, we say that a branch of $W^u(p^+)$ is positive or negative when it extends away from $p^+$ in the direction of $\mathbf{v}_u$ or $-\mathbf{v}_u$, respectively.

An orbit of $H^2$ on $W^u(p^+)$ that starts near $p^+$ and ends in $\Sigma$, is a sequence

$$\mathcal{O} = \{e_{-N}, \ldots, e_{-1}, e_0\} \quad \text{with} \quad e_{i+1} = H^2(e_i) \text{ for all } -N \le i \le -1, \tag{6}$$

that satisfies the boundary conditions

$$e_{-N} = p^+ + \delta_u \mathbf{v}_u, \tag{7}$$

$$e_0 \cdot \mathbf{n} = 0. \tag{8}$$

Here, $\delta_u$ is sufficiently small and $\mathbf{n} = (1, -1, 0)^T$ is the vector normal to $\Sigma$.

A standard approach to solving the BVP (6)–(8) is to formulate it as a single, large zero problem. Specifically, since $H$ is a three-dimensional map, this BVP comprises $3N+4$ scalar equations: $3N$ from the mapping requirement in (6), three from the boundary condition (7), and a single one from the boundary condition (8). There are also $3N + 4$ scalar unknowns: the coordinates of the $N + 1$ points $e_i \in \mathbb{R}^3$ and the scalar parameter $\delta_u$, which needs to be solved for to ensure boundary condition (8) is satisfied. Hence, this system of nonlinear equations is well posed and can be solved with Newton's method.

We implemented the BVP (6)–(8) in `Julia` and use the `Julia` function `nlsolve`. Any solution $\mathcal{O}$ found this way can readily be followed in a parameter by pseudo-arclength continuation, provided we account for the change in coordinates of the fixed point and the appropriate unit eigenvector; note that $p^+$ is known explicitly, as given by (5), and we find $\mathbf{v}_u$ numerically with the `Julia` function `eigen`, where we stipulate that its first component be positive. We used the `Julia` function `continuation(prob, PALC(), ...)` provided as part of the software package `BifurcationKit.jl` [28].

### 3.2 Finding and correcting a seed solution

A crucial step in solving the BVP (6)–(8) is to find an initial approximate orbit

$$\widetilde{\mathcal{O}} = \{\widetilde{e}_{-N}, \ldots, \widetilde{e}_{-1}, \widetilde{e}_0\},$$

as a seed to ensure that Newton's method converges to $\mathcal{O}$. Simple iterations of selected points cannot be used for this purpose, because we are dealing with saddle objects that are repelling in both forward and backward time.

Rather, we find the seed $\widetilde{\mathcal{O}}$ as a pseudo-orbit on $W^u(p^+)$. To this end, we compute the unstable manifold $W^u(p^+)$ with the algorithm from Section 2, where we impose the relatively stringent accuracy settings

$$\Delta_{\max} = 0.01, \quad \alpha_{\max} = 0.3, \quad (\Delta\alpha)_{\max} = 0.03, \quad \text{and} \quad \Delta_{\min} = 10^{-7}.$$

To find points on $W^u(p^+)$ that lie approximately in $\Sigma$ we proceed as follows. For each mesh point $q$ in the computed mesh $M$ that has a positive $x$-coordinate, we evaluate the expression $d(q) = q \cdot \mathbf{n}$ as in (8) to identify pairs for which the sign changes; note that $d$ represents the (signed) distance of $q$ from the section $\Sigma$. From such pairs, we select the mesh point closest to $\Sigma$, which we refer to as $\widetilde{a}_0 = q_{\ell_0}$. We construct its pseudo-orbit (2) by

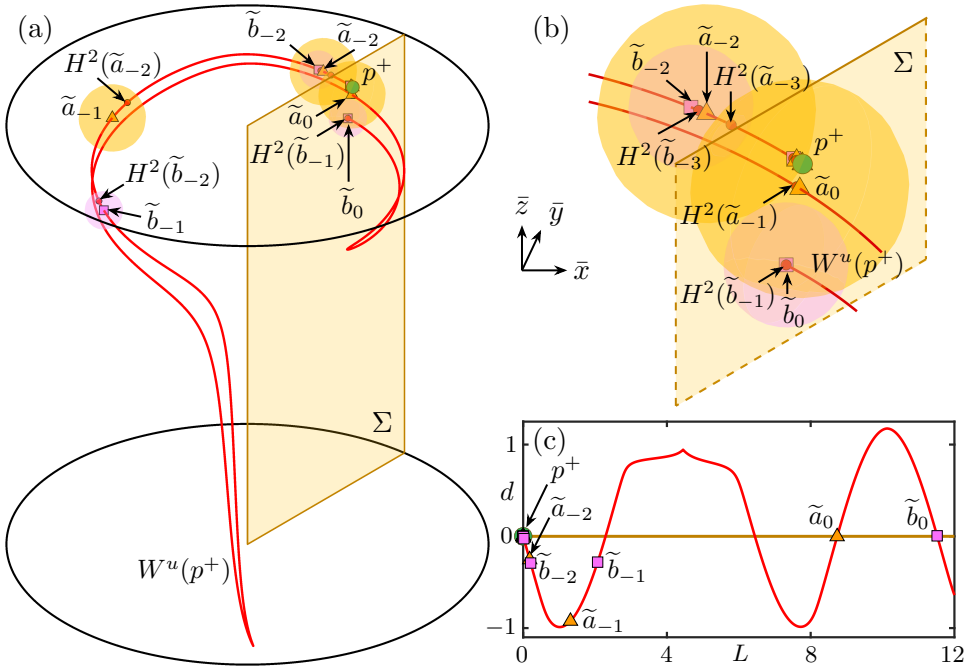


Figure 3: Seeds for the first and second intersections of the negative branch of $W^u(p^+)$ (red curve) with $\Sigma$ (yellow plane), constructed as pseudo-orbits $\{\widetilde{a}_i\}_{-8\le i\le 0}$ (orange triangles) and $\{\widetilde{b}_i\}_{-8\le i\le 0}$ (pink squares) under $H^2$ (with $\alpha = 4.2$, $\beta = -0.3$, and $\xi = 0.8$). The last three $\varepsilon$-balls of each pseudo-orbit are displayed (yellow balls of radius 0.14 around $\widetilde{a}_i$, pink balls of radius 0.08 around $\widetilde{b}_i$), which contain $H^2(\widetilde{a}_i)$ and $H^2(\widetilde{b}_i)$ (red points), respectively. Panel (a) shows these objects in $\mathcal{C}$; panel (b) is an enlargement near $\widetilde{a}_0$ and $\widetilde{b}_0$; and panel (c) shows the distance $d(q)$ along the branch of $W^u(p^+)$ versus arclength $L$, with the values for $\{\widetilde{a}_i\}$ and $\{\widetilde{b}_i\}$ labelled.

following the respective integer pointers. Hence, we use as seed the pseudo-orbit of length $K+1$ given by

$$\widetilde{\mathcal{O}} = \{\widetilde{a}_{-K}, \ldots, \widetilde{a}_{-1}, \widetilde{a}_0\} = \{q_{\ell_K}, q_{\ell_{K-1}}, \ldots, q_{\ell_1}, q_{\ell_0}\}.$$

This choice of seed is illustrated in Fig. 3 for the negative branch of $W^u(p^+)$, which is visualised up to its second intersection with $\Sigma$. Also shown are the pseudo-orbits $\{\widetilde{a}_i\}_{-8\le i\le 0}$ up to the point $\widetilde{a}_0$ nearest the first, and $\{\widetilde{b}_i\}_{-8\le i\le 0}$ up to $\widetilde{b}_0$ nearest the second intersection with $\Sigma$. Balls of radius 0.14 and 0.08 around the last three points of the respective orbit illustrate that these are $\varepsilon$-pseudo-orbits for $H^2$. Panel (a) of Fig. 3 shows these objects in the compactified cylinder $\mathcal{C}$. Observe how the negative branch of $W^u(p^+)$ makes an excursion towards large negative $\bar{z}$, before intersecting $\Sigma$ near $\widetilde{a}_0$, turning around and intersecting $\Sigma$ for the second time near $\widetilde{b}_0$. An enlargement near the points $p^+$, $\widetilde{a}_0$ and $\widetilde{b}_0$ is shown in panel (b). How the points $\widetilde{a}_0$ and $\widetilde{b}_0$ are found is illustrated in Fig. 3(c), where we plot $d(q)$ as a function of the arclength $L$ of the computed branch. Note that the first two crossings of the $L$ axis are for $x < 0$ and, hence, do not represent intersections with the half-plane $\Sigma$.

Figure 4 illustrates the orbit segments $\{a_i\}_{-8\le i\le 0}$ and $\{b_i\}_{-8\le i\le 0}$ that have been corrected with Newton's method from the seeds $\{\tilde{a}_i\}_{-8\le i\le 0}$ and $\{\tilde{b}_i\}_{-8\le i\le 0}$. Panel (a) shows the two orbits in the compactified cylinder $\mathcal{C}$ with $p^+$, $W^u(p^+)$ and $\Sigma$, and panel (b) is an

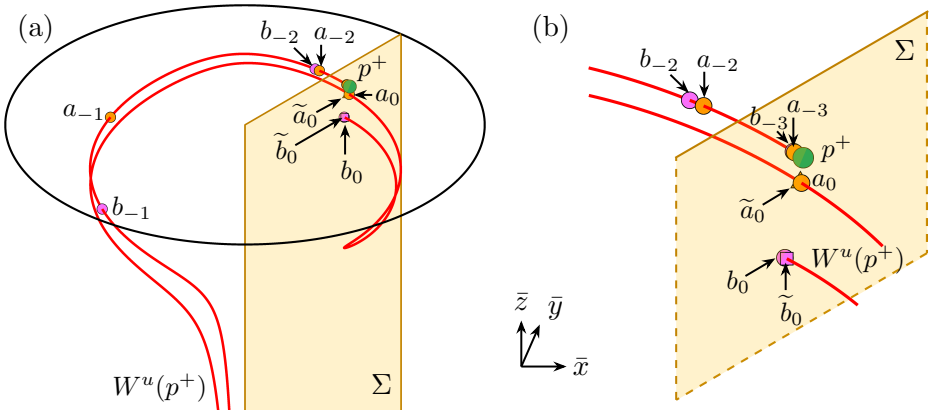


Figure 4: The resulting Newton-corrected orbits $\{a_i\}_{-8\le i\le 0}$ (yellow points) and $\{b_i\}_{-8\le i\le 0}$ (pink points) that satisfy the BVP (6)–(8) for the first and second intersection points of negative branch of $W^u(p^+)$ (red curve) with $\Sigma$ (yellow plane), respectively. Panel (a) shows the situation in $\mathcal{C}$, and panel (b) is an enlargement near $a_0$ and $b_0$; compare with Fig. 3.

enlargement near $p^+$, $a_0$ and $b_0$; compare with Fig. 3. Also shown are the initial mesh points $\widetilde{a}_0$ and $\widetilde{b}_0$, which are already very close to the corrected points $a_0, b_0 \in \Sigma$; indeed, $W^u(p^+)$ was computed here with a high mesh resolution.

### 3.3 Continuing intersection points in one parameter

A significant advantage of computing points in $W^u(p^+) \cap \Sigma$ in the form of orbits that solve the BVP (6)–(8) is that we can continue any such solution in parameters. As an example, we treat $\xi$ as a free parameter (while keeping $\alpha$ and $\beta$ fixed) and continue the intersection points as entire orbit segments on $W^u(p^+)$. Following the notation in [5], we denote by $w^+(\ell;\xi)$ the $\ell$th intersection point of $W^u(p^+)$ with $\Sigma$ at the given parameter value $\xi$, where the index $\ell \in \mathbb{Z}\setminus\{0\}$ is positive for the positive branch and negative for the negative branch. We already found the two points $w^+(-1;0.8) = a_0$ and $w^+(-2;0.8) = b_0$, and many more, on both branches, can be found in the same way.

We consider the range $\xi \in [0.01, 0.99]$ and compute all $\xi$-parametrised curves of intersection points, that is, we compute the family

$$\boldsymbol{w}^+(\ell) := \{w^+(\ell;\xi) \mid \xi \in [0.01, 0.99]\}.$$

Our computational set-up automatically computes each curve, starting from $\xi = 0.8$, by successively selecting all values of $\ell$ from a given (finite) index set. In combination with the automated detection of the required seeds, this continuation approach is considerably more efficient and accurate than the method employed in [5, 10], where many intersection points over a fine grid of $\xi$-values were found by interpolation and then rendered, again by interpolation, as $\xi$-dependent curves.

We computed $\xi$-parametrised curves $\boldsymbol{w}^+(\ell)$ with $0 < |\ell| \le 2^{11}$. For each fixed value of $\ell$, pseudo-arclength continuation was performed with initial step size $ds = 10^{-3}$, minimum step size $ds_{\min} = 10^{-4}$, and maximum step size $ds_{\max} = 10^{-3}$. The resulting $2^{12}$ curves are shown in Fig. 5 in terms of their $\bar{z}$-values. Most curves $\boldsymbol{w}^+(\ell)$ are coloured dark ($\ell > 0$)

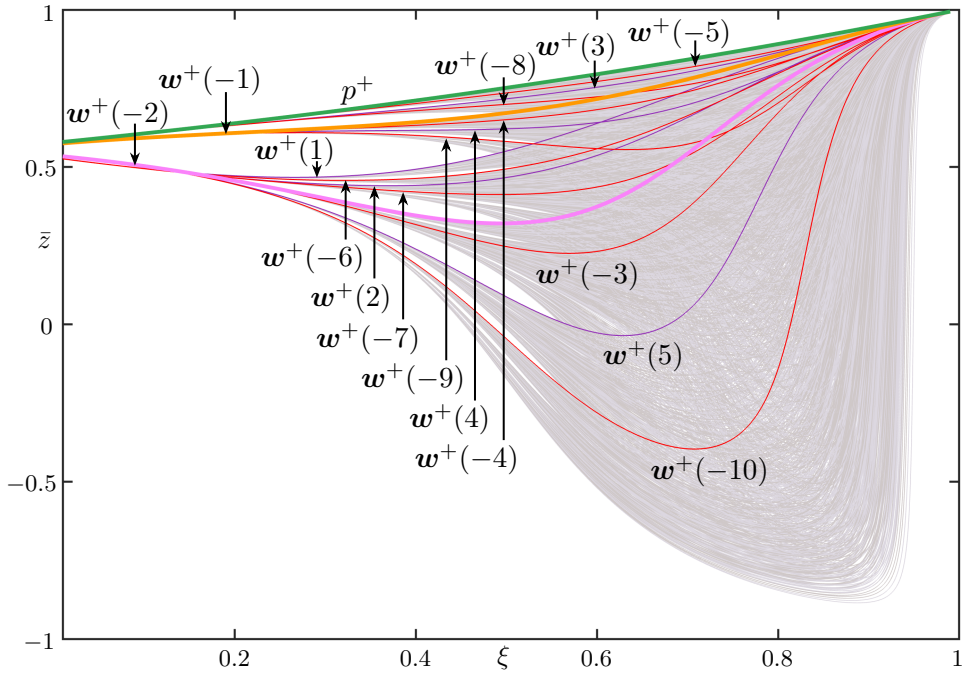


Figure 5: The continued $\xi$-parametrised intersection curves $\boldsymbol{w}^+(\ell)$ of points in $W^u(p^+) \cap \Sigma$ for $0 < |\ell| \leq 2^{11}$, shown in the $(\xi, \bar{z})$-plane, together with $p^+$ (green). Highlighted are the curves $\boldsymbol{w}^+(-1)$ (orange) and $\boldsymbol{w}^+(-2)$ (pink), as well as those for $\ell = -3, \ldots, -10$ (red) and $\ell = 1, \ldots, 5$ (purple); all other curves are shown in light grey when $\ell < 0$ and dark grey when $\ell > 0$.

or light ($\ell < 0$) grey, with true colours only assigned when $\ell = \pm 1, \ldots, \pm 5$, as well as $\ell = -6, \ldots, -10$; also shown is the $\bar{z}$-value of $p^+$, which forms the upper boundary of all curves. The curves $\boldsymbol{w}^+(-1)$ and $\boldsymbol{w}^+(-2)$ were continued from the points $w^+(-1; 0.8) = a_0$ and $w^+(-2; 0.8) = b_0$ from Fig. 3. Note that these two curves are the lower bounds for visible gaps that appear approximately when $\xi < 0.5$. The other highlighted curves in Fig. 5 have been selected and labelled because, likewise, they are lower boundaries of such gaps. The capability to continue the curves $\boldsymbol{w}^+(\ell)$ reliably as functions of $\xi$ is a key tool for studying how and when the gaps close as $\xi$ increases. For $\xi$ sufficiently close to 1, the curves $\{\boldsymbol{w}^+(\ell)\}$ fill a solid region in the $(\xi, \bar{z})$-plane. The latter is strong evidence that $W^u(p^+)$ has the carpet property and, therefore, the hyperbolic set $\Lambda$ (containing $p^+$) is a blender. Due to its shape, we also refer to the representation in Fig. 5 as the 'carpet of carpets' [5, 10].

We remark that intersection points with $\Sigma$ of the unstable manifolds of the other fixed point $p^-$ and/or of selected periodic points in $\Lambda$ can be found in the same way. Moreover, their corresponding orbits can also be continued as curves, not just with respect to $\xi$, but also with respect to any other system parameter. How this enhanced capability can be brought to bear in the further analysis of the Hénon-like family $H$ is the subject of ongoing research.

# 4 Finding transverse and non-transverse connecting orbits

Homoclinic and heteroclinic orbits of fixed points and/or periodic orbits are intersections of their respective stable and unstable manifolds. Such connecting orbits are closely associated with recurrent dynamics that underly and organise chaotic behaviour of different kinds [3, 24]. Depending on the dimensions of the invariant manifolds involved and the nature of their intersection, the resulting connecting orbit may be transverse, that is, structurally stable, or non-transverse and, hence, break under small perturbations. Examples of the latter are homoclinic tangencies and heterodimensional cycles, which are particularly interesting as they are the primary mechanism for generating persistent non-hyperbolic dynamics [2, 7, 20].

Connecting orbits are global objects that are generally not known analytically and, therefore, need to be computed with dedicated numerical methods. We find an (approximate) connecting orbit as the solution of a BVP that defines an orbit from near one fixed point to near the same or another fixed point; see [1, 9] for examples of this approach for planar maps. Crucially, our method for finding pseudo-orbits along one-dimensional invariant manifolds of a three-dimensional diffeomorphism can be used to solve the problem of finding suitable initial guesses—for both transverse and non-transverse connecting orbits—that converge to solutions of the respective BVP set-up.

Specifically, we consider the diffeomorphism of $\mathbb{R}^3$ given by

$$T(x, y, z) = (z + k\,[x^2 + y^2 - 2],\, x,\, y),$$

where $k \in \mathbb{R}$ is a parameter. This map is part of a larger class of quadratic volume-preserving maps studied in [22], and was first explicitly investigated in [21] for $k = \sqrt{20}$. Unless otherwise stated, we also fix $k = \sqrt{20}$ as in [21] to demonstrate our approach to finding homoclinic and heteroclinic (and heterodimensional) connections.

The map $T$ combines a nonlinear shear on $x$ with a rotation of the three coordinates, and it is reversible: $T$ is invariant under the transformation

$$R(x, y, z) = (-z, -y, -x)$$

in conjunction with the reversal of (discrete) time. As a result, any fixed points and periodic orbits come in symmetric pairs with complementary stability properties. The map $T$ has the two hyperbolic fixed points

$$p^+ = (1, 1, 1) \qquad \text{and} \qquad p^- = (-1, -1, -1) = R(p^+),$$

which exists for all $k \geq 0$, as well as the two hyperbolic period-three orbits

$$\begin{aligned} q^+ &= \{q_1^+, q_2^+, q_3^+\} = \{(1, -1, -1),\, (-1, 1, -1),\, (-1, -1, 1)\} \text{ and} \\ q^- &= \{q_1^-, q_2^-, q_3^-\} = \{\quad (-1, 1, 1),\quad (1, -1, 1),\quad (1, 1, -1)\} = R(q^+), \end{aligned}$$

which exists for all $k > 1$. Note that these eight points lie at the corners of a cube, irrespective of the value of $k$.

We focus on the two fixed points and the one-dimensional unstable manifold $W^u(p^+)$ and one-dimensional stable manifold $W^s(p^-)$. Since $W^s(p^-) = R(W^u(p^+))$, it suffices to compute $W^u(p^+)$ with the method from Section 2 and, when required, obtain $W^s(p^-)$ by

applying $R$ to the computed mesh. As was the case in Section 3, it is important and practical to compactify phase space. We rescale $\mathbb{R}^3$ to the open unit ball $\mathbb{B}^3$ via the transformation

$$\mathcal{C}(x,y,z) = (\bar{x},\bar{y},\bar{z}) = \frac{(x,y,z)}{1+\sqrt{(1+\|(x,y,z)\|^2)}},$$

with the action of $T$ on $\mathbb{B}^3$ given by $\mathcal{C}\circ T\circ \mathcal{C}^{-1}$. To keep the notation simple, we again refer to the conjugate map as $T$, and use the same labels for its invariant objects.

### 4.1 BVP formulation of homoclinic orbits

We now show how to find homoclinic orbits to $p^+$. The BVP set-up for this type of connecting orbit is similar to that described in Section 3.1. We consider an orbit

$$\mathcal{O} = \{e_{-N},\ldots,e_{-1},e_0\} \quad \text{with} \quad e_{i+1} = T(e_i) \text{ for all } -N \le i \le -1. \tag{9}$$

As before, we stipulate that $e_{-N}$ lies on $W^u(p^+)$ near $p^+$, but for the final point $e_0$, we now require that it lies in the two-dimensional stable linear eigenspace of $p^+$. This is expressed by the boundary conditions

$$e_{-N} = p^+ + \delta_u \mathbf{v}_u, \tag{10}$$
$$e_0 = p^+ + \delta_s \mathbf{v}_s + \delta_{ss}\mathbf{v}_{ss}, \tag{11}$$

where $\mathbf{v}_u$ is the (unit) unstable eigenvector, and $\mathbf{v}_s$ and $\mathbf{v}_{ss}$ are the (unit) weak and strong stable eigenvectors of the Jacobian matrix $DT(p^+)$; this formulation of the boundary condition can be interpreted as a version of projection boundary conditions [1]. The real parameters $\delta_u$, $\delta_s$ and $\delta_{ss}$ are solved for as part of the overall BVP; they control the distances from $p^+$ to $e_{-N}$ and $e_0$ along the respective eigenvectors. These three parameters all need to be suitably small to ensure that $\mathcal{O}$, indeed, represents a homoclinic orbit to $p^+$. Note that the BVP (9)–(11) is well posed, featuring $3N+3+3$ equations for the $3(N+1)+3$ unknowns.

### 4.2 Constructing a homoclinic pseudo-orbit as a seed

To find a seed solution for a homoclinic orbit to $p^+$, we first compute the one-dimensional unstable manifold $W^u(p^+)$ with the algorithm from Section 2; we set the accuracy parameters to

$$\Delta_{\max} = 0.1, \quad \alpha_{\max} = 0.3, \quad (\Delta\alpha)_{\max} = 10^{-3}, \quad \text{and} \quad \Delta_{\min} = 10^{-6}.$$

We then use this data to construct a pseudo-orbit that can serve as a seed solution for the BVP (9)–(11).

Figure 6 presents an example, where we consider $W^u(p^+)$ only up to arclength $L = 20$. We now consider the distance of points on $W^u(p^+)$ to $p^+$, which we also refer to as $d$; it is shown in panel (a) as a function of $L$. Any local minimum of $d$ corresponds to a close pass of $W^u(p^+)$ past $p^+$ and, hence, to a possible (approximate) end point of a homoclinic orbit; note that $d$ is shown on a logarithmic scale. We select the smallest minimum, at $L \approx 16.922$, as the point $\widetilde{a}_0 = q_{\ell_0}$, and then construct its pseudo-orbit $\{\widetilde{a}_j\}_{-13\le j\le 0}$ as explained in Section 2.2; the first point $\widetilde{a}_{-13}$ practically lies at $p^+$ (with $\|\widetilde{a}_{-13}-p^+\| < 0.05$).

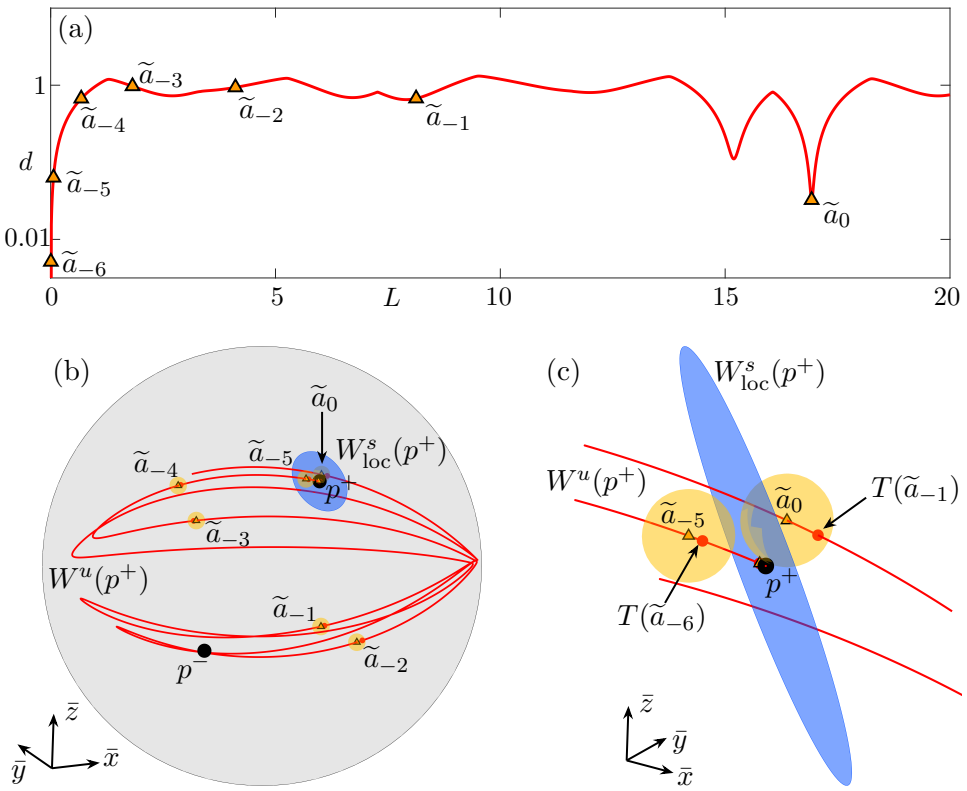


Figure 6: Identifying a pseudo-orbit $\{\widetilde{a}_j\}_{-13\le j\le 0}$ (orange triangles) of $T$ as a seed for a homoclinic orbit to $p^+$. Panel (a) shows on a logarithmic scale the distance $d$ to $p^+$ of points along $W^u(p^+)$ (red curve) versus their arclength $L$; its smallest local minimum up to $L = 20$ defines the point $\widetilde{a}_0$. Panel (b) shows these objects in compactified coordinates with $W^s_{\mathrm{loc}}(p^+)$ (blue disk) and images $T(\widetilde{a}_j)$ (red points) that lie in $\varepsilon$-balls (yellow) with $\varepsilon = 0.03$ around $\widetilde{a}_{j+1}$; and panel (c) is an enlargement near $p^+$ (black point).

The location of $\{\widetilde{a}_j\}_{-13\le j\le 0}$ in $\mathbb{B}^3$ is shown in Fig. 6(b). Here, the local stable manifold $W^s_{\mathrm{loc}}(p^+)$ is represented by a small disk in the plane spanned by $\mathbf{v}_s$ and $\mathbf{v}_{ss}$. For each point $\widetilde{a}_j$ in the pseudo-orbit we find $\|T(\widetilde{a}_j) - \widetilde{a}_{j+1}\| < 0.03$, which is illustrated by the $\varepsilon$-balls of radius $\varepsilon = 0.03$ centred at $\widetilde{a}_j$. Note in the enlargement near $p^+$, shown in panel (c), that $T(\widetilde{a}_{-1})$ lies in the $\varepsilon$-ball centred at $\widetilde{a}_0$, and likewise for $T(\widetilde{a}_{-6})$ and $\widetilde{a}_{-5}$. The defining point $\widetilde{a}_0$ satisfies $\|\widetilde{a}_0 - p^+\| \approx d(16.922) \approx 0.0324$, so is quite close to $p^+$ but does not actually lie in the linear approximation of $W^s_{\mathrm{loc}}(p^+)$.

We found that Newton's method does converge if we use the pseudo-orbit $\{\widetilde{a}_j\}_{-13\le j\le 0}$ as a seed for solving the BVP (9)–(11). However, the finite orbit only represents an accurate connecting orbit if the internal parameters $\delta_u$, $\delta_s$ and $\delta_{ss}$ in (10) and (11) are sufficiently small; only then will the linear eigenspace be a good approximation of the respective invariant manifold [1, 16]. By construction of the pseudo-orbit, $\delta_u$ is sufficiently small, but correcting $\widetilde{a}_0$ to satisfy boundary condition (11) result in arguably too large values for $\delta_s$ and $\delta_{ss}$. To obtain a seed solution that does not have this issue, we extend the pseudo-orbit $\{\widetilde{a}_j\}_{-13\le j\le 0}$ by adding points to its tail that are successively closer to $p^+$. To this end, we

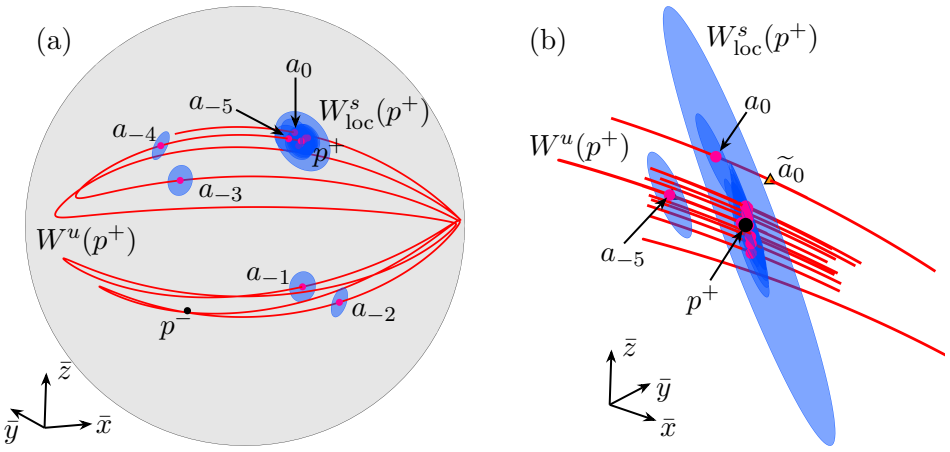


Figure 7: The homoclinic orbit to $p^+$ found as the solution $\{a_j\}_{-13\le j\le 8}$ (magenta dots) to the BVP (9)–(11) with the extension $\widetilde{\mathcal{O}} = \{\widetilde{a}_j\}_{-13\le j\le 8}$ of the pseudo-orbit from Fig. 6 as seed. At each point $a_j$, the manifolds $W^u(p^+)$ (red curve) and $W^s(p^+)$ (shown locally as blue disks) intersect. Panel (a) shows these objects in compactified coordinates and panel (b) is an enlargement near $p^+$ (black point). Compare with Figs. 6(b) and 6(c).

invoke the action of the linearisation $DT(p^+)$ and define

$$\widetilde{a}_j := p^+ + (\lambda_s)^j\,(\widetilde{a}_0 - p^+) \text{ for } 1 \le j \le 8,$$

where $\lambda_s \approx -0.7887$ is the weak stable eigenvalue. This definition encodes slow contraction towards $p^+$ along the weak stable direction, which is a good approximation of the nonlinear action of $T$ in a neighbourhood of $p^+$. The extended pseudo-orbit of length 22 is then given by

$$\widetilde{\mathcal{O}} = \{\widetilde{e}_i\}_{-21\le i\le 0} = \{\widetilde{a}_j\}_{-13\le j\le 8}, \tag{12}$$

where now $\|\widetilde{e}_0 - p^+\| = \|\widetilde{a}_8 - p^+\| < 0.005$.

We apply Newton's method with the extended pseudo-orbit $\widetilde{\mathcal{O}}$ from (12) as seed. The converged solution $\{a_j\}_{-13\le j\le 8}$ satisfies the BVP (9)–(11) with $\delta_u < 0.005$ for $a_{-13}$ in boundary condition (10) and $\delta_s, \delta_{ss} < 0.05$ for $a_8$ in boundary condition (11). Figure 7 illustrates this computed homoclinic orbit in $\mathbb{B}^3$, in a global view in panel (a) and in an enlargement near $p^+$ in panel (b); compare with Figs. 6(b) and 6(c). In Fig. 7, small disks represent the linear approximations of the two-dimensional manifold $W^s(p^+)$ locally at each of the homoclinic points $a_j$; these are obtained by propagating the stable eigenvectors under the linearisation $DT$. Panel (b) also shows the defining point $\widetilde{a}_0$ of the pseudo-orbit, which has been corrected to the point $a_0$. Note that all points $a_j$ with $1 \le j \le 8$ lie very close to the linear eigenspace of $p^+$. This constitutes visual confirmation that $\{a_j\}_{-13\le j\le 8}$ is an accurate approximation of an actual homoclinic orbit to $p^+$.

The homoclinic orbit visualised in Fig. 7 is not unique. Other homoclinic orbits to $p^+$ can be found in a similar way by considering $W^u(p^+)$ up to larger arclength. This is illustrated in Fig. 8, where we consider $W^u(p^+)$ up to arclenth $L = 170$ and selected the three smallest local minima of the distance function $d$: they define (in order of increasing values of $d$) the points $\widetilde{b}_0$ at $L \approx 126.582$, $\widetilde{c}_0$ at $L \approx 155.070$, and $\widetilde{d}_0$ at $L \approx 98.357$. In fact,

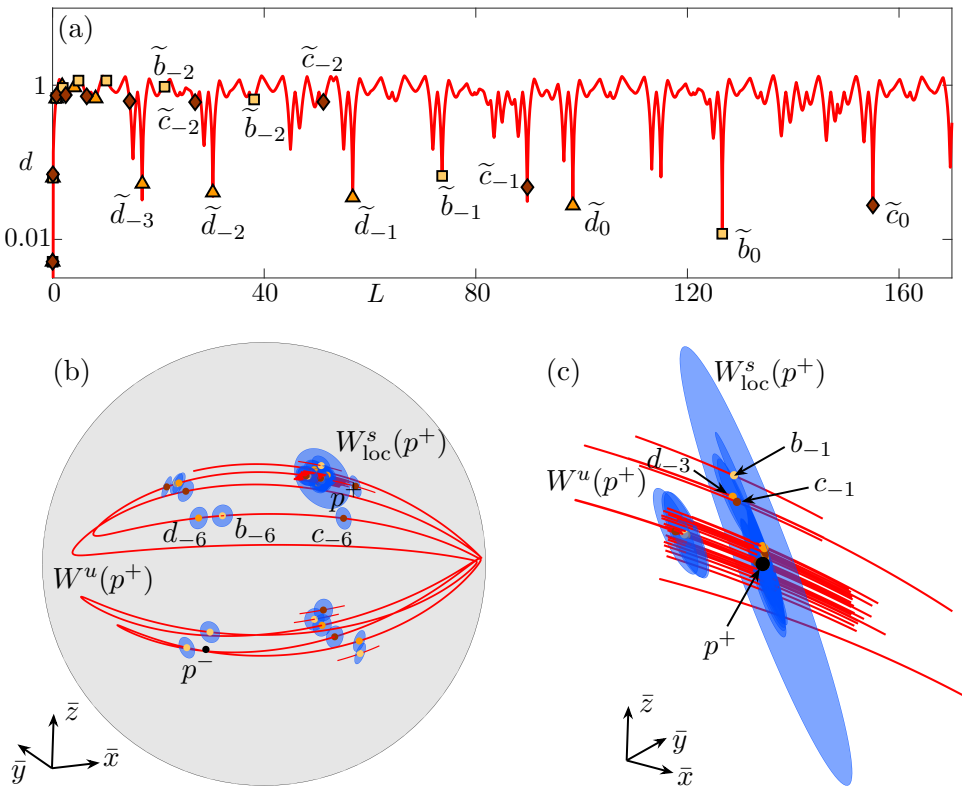


Figure 8: Three additional homoclinic orbits of $T$ to $p^+$. Panel (a) identifies pseudo-orbits $\{\widetilde{b}_j\}_{-15\le j\le 5}$ (yellow squares), $\{\widetilde{c}_j\}_{-15\le j\le 5}$ (brown diamonds) and $\{\widetilde{d}_j\}_{-15\le j\le 5}$ (orange triangles) as local minima of $d(L)$. Panel (b) and the enlargement near $p^+$ in panel (c) show the corresponding homoclinic orbits $\{b_j\}_{-15\le j\le 5}$, $\{c_j\}_{-15\le j\le 5}$, and $\{d_j\}_{-15\le j\le 5}$ in $\mathbb{B}^3$ with matching colours, together with local linear segments of $W^u(p^+)$ (red) and disks of $W^s(p^+)$ (blue); compare with Figs. 6(a) and 7.

these three mesh points lie in a single fundamental domain of $W^u(p^+)$ and, therefore, lie on three distinct orbits. As before, we construct three pseudo-orbits and extend them to near $p^+$ to obtain the seeds $\{\widetilde{b}_j\}_{-15\le j\le 5}$, $\{\widetilde{c}_j\}_{-15\le j\le 5}$, and $\{\widetilde{d}_j\}_{-15\le j\le 5}$ for the BVP (9)–(11). Each of the three seed solutions converges to an approximate homoclinic orbit, denoted $\{b_j\}_{-15\le j\le 5}$, $\{c_j\}_{-15\le j\le 5}$, and $\{d_j\}_{-15\le j\le 5}$, respectively. They are presented in Fig. 8(b) in the style of Figure 7, with $W^u(p^+)$ shown as a curve for $L \le 20$, together with local segments of $W^u(p^+)$ and disks of $W^s(p^+)$ at each homoclinic point. The enlargement near $p^+$ in Fig. 8(c) shows that, effectively, the tails with $1 \le j \le 5$ of all three homoclinc orbits already lie on the linearisation of $W^s_{\rm loc}(p^+)$, which is again a confirmation of the accuracy of these computations.

The homoclinic orbits $\{b_j\}_{-15\le j\le 5}$ and $\{c_j\}_{-15\le j\le 5}$ have further excursions away from $p^+$ than $\{d_j\}_{-15\le j\le 5}$. This can be seen in Fig. 8(a): already $\widetilde{b}_{-2}$ and $\widetilde{c}_{-2}$ lie at $O(1)$ distance from $p^+$, while $\widetilde{d}_{-2}$ and even $\widetilde{d}_{-3}$ remain of order $O(10^{-2})$ close to $p^+$; notice also that the short disjoint segments of $W^u(p^+)$ in Fig. 8(b) (bottom right) only pass through homoclinic points from $\{b_j\}_{-15\le j\le 5}$ and $\{c_j\}_{-15\le j\le 5}$. Upon further inspection, we find that, in fact, the homoclinic orbit $\{d_j\}_{-15\le j\le 5}$ is actually the same as the one shown in Figure 7. Indeed,

$\widetilde{d}_{-3}$ effectively lies at the same local minimum at $L \approx 16.922$ that we used to identify $\widetilde{a}_0$; compare Figs. 8(a) and 6(a). Indeed, the corrections $a_0$ and $d_{-3}$ are equal to within the computed accuracy, which can be inferred when comparing Figs. 8(b) and 7(a). In fact, $\|a_j - d_{j-3}\| < 10^{-10}$ for all $j$ where both points exist, which means that they both represent the same homoclinic orbit. This issue that different minima may give the same homoclinic orbit can be dealt with by comparing the computed representations, or by ensuring that the chosen seeds all lie in a single fundamental domain.

We remark that the same approach can be used to find transverse heteroclinic orbits formed by a one-dimensional invariant manifold between two different saddle fixed or periodic points. To this end, boundary condition (11) is replaced by the equivalent boundary condition for the stable manifold at the other saddle point, and the distance function $d(L)$ defined accordingly.

### 4.3 BVP formulation of a non-transverse heterdimensional orbit

A heterodimensional cycle of a diffeomorphism consists of a non-transverse connection between two fixed points of different unstable dimensions, as well as a transverse return connection. We now show how a non-transverse heterodimensional orbit of the map $T$ between its two fixed points $p^+$ and $p^-$ can be found. This connecting orbit lies at the intersection of the one-dimensional invariant manifolds $W^u(p^+)$ and $W^s(p^-)$, which we also formulate as a BVP with appropriate projection boundary conditions. More precisely, we consider an orbit of length $N_u + N_s + 1$ of the form

$$\begin{array}{rcl} \mathcal{O} & = & \{e_{-N_u}, \ldots, e_{-1}, e_0, e_1, \ldots, e_{N_s}\} \text{ with} \\ e_{i+1} & = & T(e_i) \text{ for all } -N_u \leq i < N_s, \end{array} \tag{13}$$

which we require to lie on both $W^u(p^+)$ and $W^s(p^-)$. This is achieved by imposing the boundary conditions:

$$e_{-N_u} = p^+ + \delta_u^+ \mathbf{v}_u^+, \tag{14}$$

$$e_{N_s} = p^- + \delta_s^- \mathbf{v}_s^-, \tag{15}$$

where $\mathbf{v}_u^+$ is the single unstable eigenvector of $p^+$, and $\mathbf{v}_s^-$ is the single stable eigenvector of $p^-$. A solution to the BVP (13)–(15) is an approximation of a non-transverse heterodimensional connection between $p^+$ and $p^-$ when the internal parameters $\delta_u^+$ and $\delta_s^-$ are sufficiently small. Note that condition (14) is the same as (10), but the notation now distinguishes the respective eigenvalues and eigenvectors of the two fixed points. The two real parameters $\delta_u^+$ and $\delta_s^-$ are included in the $3(N_u + N_s + 1) + 2$ unknowns of the overal BVP (13)–(15), which constitutes $3(N_u + N_s) + 3 + 3$ equations. Hence, one free parameter is required to ensure the BVP has a unique (isolated) solution. In our context, the single parameter $k$ of $T$ needs to be varied and solved for in order to find the non-transverse heterodimensional connection, which is of codimension one.

### 4.4 Constructing a non-transverse heterodimensional connecting pseudo-orbit as a seed

The key for finding a solution of the BVP (13)–(15) is again the construction of a successful seed. This is a difficult task because two curves in $\mathbb{R}^3$ do not necessarily come close to

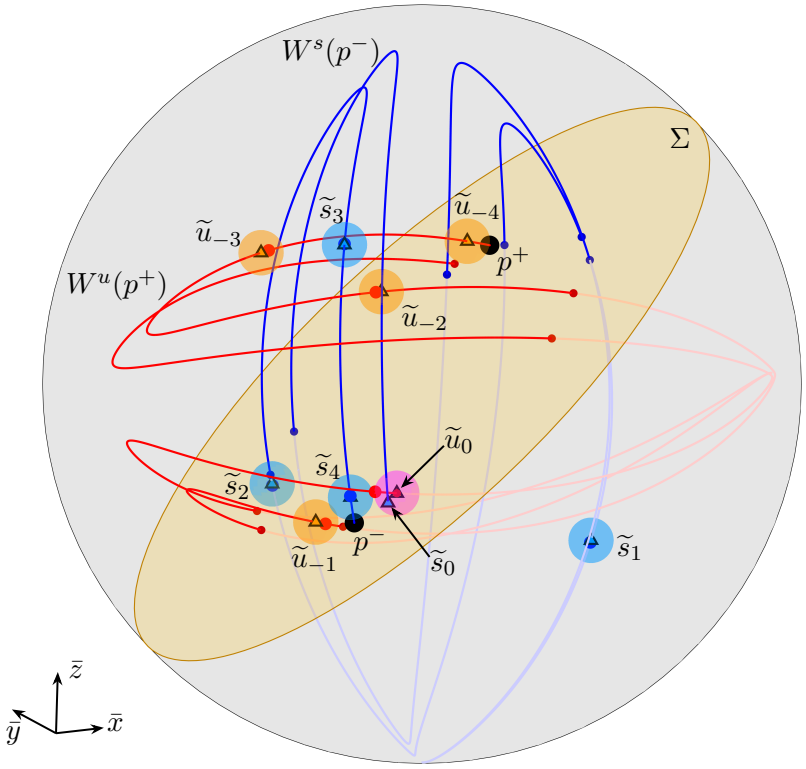


Figure 9: Construction of a seed for a non-transverse heterdimensional orbit of $T$ between $p^+$ and $p^-$ in $\mathbb{B}^3$. The one-dimensional manifolds $W^u(p^+)$ (red curve) and $W^s(p^-)$ (blue curve) intersect the plane $\Sigma$ (yellow) at the small red and blue points, respectively; the two manifolds are shown fainter below $\Sigma$. Two pseudo-orbits $\{\widetilde{u}_j\}$ on $W^u(p^+)$ (orange triangles and balls containing preimages) and $\{\widetilde{s}_j\}$ on $W^s(p^-)$ (light-blue trianges and balls containing preimages) end at the points $\widetilde{u}_0, \widetilde{s}_0 \in \Sigma$, respectively, which lie in the same (magenta) $\varepsilon$-ball. Their concatenation is a successful seed solution for the BVP (13)–(15).

each other. We take an approach that is motivated by Lin's method for finding connecting orbits [19]. We consider the intersection sets of $W^u(p^+)$ and $W^s(p^-)$ with a chosen plane $\Sigma$ to identify two points, one from either intersection set, that are close to each other in $\Sigma$. Their respective pseudo-orbits define a heterodimensional connecting pseudo-orbit from $p^+$ to $p^-$ as seed. As before, we apply Newton's method to the defining BVP to yield a true orbit, which can be interpreted as closing all $\varepsilon$-gaps of the seed.

Figure 9 illustrates this approach. The one-dimensional manifolds $W^u(p^+)$ and $W^s(p^-)$ are shown up to arclength $L = 10.25$ in $\mathbb{B}^3$, together with the plane

$$\Sigma := \{(\bar{x}, \bar{y}, \bar{z}) \in \mathbb{B}^3 : \bar{x} = \bar{z}\},$$

which contains $p^+$ and $p^-$, and the intersection sets $W^u(p^+) \cap \Sigma$ and $W^s(p^-) \cap \Sigma$. The two mesh points $\widetilde{u}_0 \in W^u(p^+)$ and $\widetilde{s}_0 \in W^s(p^-)$ are closest to two corresponding intersection points that lie near each other in $\Sigma$. In fact, $\|\tilde{u}_0 - \tilde{s}_0\| < \varepsilon = 0.03$, and the we show in Figure 9 $\varepsilon$-balls of radius $\varepsilon = 0.03$ at each of the points of the corresponding pseudo-orbits $\{\widetilde{u}_i\}_{-14 \le i \le 0}$ and $\{\widetilde{s}_i\}_{0 \le i \le 14}$ on $W^u(p^+)$ and $W^s(p^-)$, respectively, which were obtained as

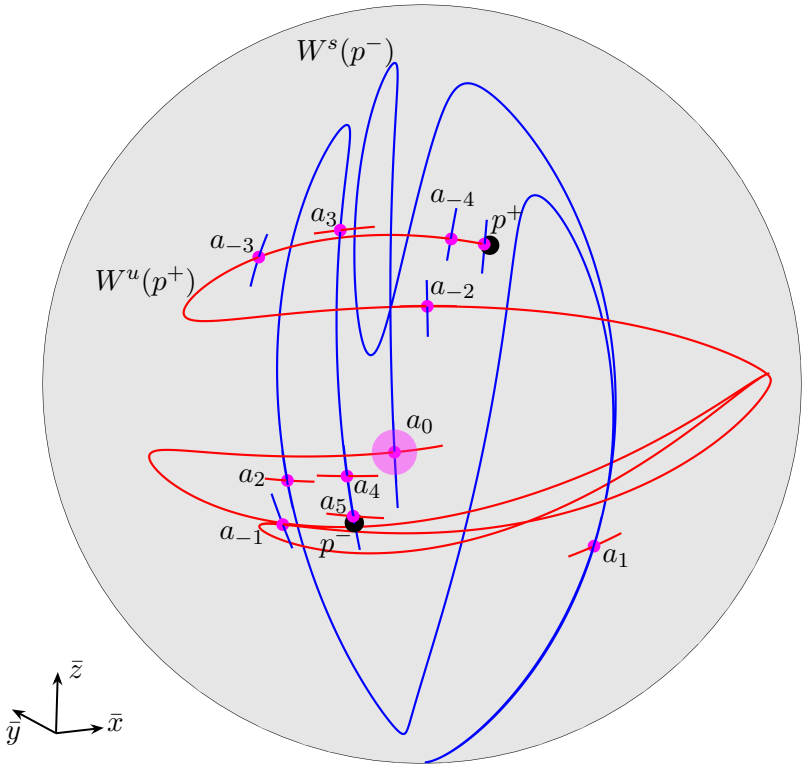


Figure 10: The non-transverse heterodimensional connecting orbit $\{a_j\}_{-14\le j\le 14}$ of $T$ from $p^+$ to $p^-$ that is found as a solution of the BVP (13)–(15) with $k \approx 2.81$. Shown in $\mathbb{B}^3$ are $W^u(p^+)$ (red curve) and $W^s(p^-)$ (blue curve) up to arclength $L = 9.5$ (just past their intersection point $a_0$ highlighted by a magenta ball), as well as local approximations of these manifolds at each point $a_j$; compare with Fig. 9.

in Section 3.2; also shown is an $\varepsilon$- ball that contains $\widetilde{u}_0$ and $\widetilde{s}_0$. Concatenation of the two pseudo-orbits results in the heterodimensional connecting pseudo-orbit

$$\widetilde{\mathcal{O}} = \{\widetilde{e}_{-N_u}, \ldots, \widetilde{e}_{N_s}\} = \{\widetilde{u}_{-14}, \ldots, \widetilde{u}_{-1}, \widetilde{u}_0, \widetilde{s}_1, \ldots, \widetilde{s}_{14}\}. \tag{16}$$

with $N_u = N_s = 14$. Note that the choice of $\widetilde{e}_0 = \widetilde{u}_0$ as the midpoint is for definiteness and not significant; we could equally have chosen $\widetilde{s}_0$ or the average of the two points, instead.

The heterodimensional connecting pseudo-orbit $\widetilde{\mathcal{O}}$ defined by (16) is indeed a good seed for the non-transverse heterodimensional orbit that solves the BVP (13)–(15). Newton's method converges to the solution $\{a_j\}_{-14\le j\le 14}$ from $p^+$ to $p^-$ that is shown in Fig. 10. As part of this iterative process, the parameter $k$ has changed from $k = \sqrt{20} \approx 4.47$ to the specific value $k \approx 2.81$, at which this non-transverse heterodimensional connecting orbit exists. Note that the two segments of the overall orbit are now 'glued together' at the central point $a_0 \in W^u(p^+) \cap W^s(p^-)$; in other words, the 'Lin gap' between $\widetilde{u}_0$ and $\widetilde{s}_0$ has been closed.

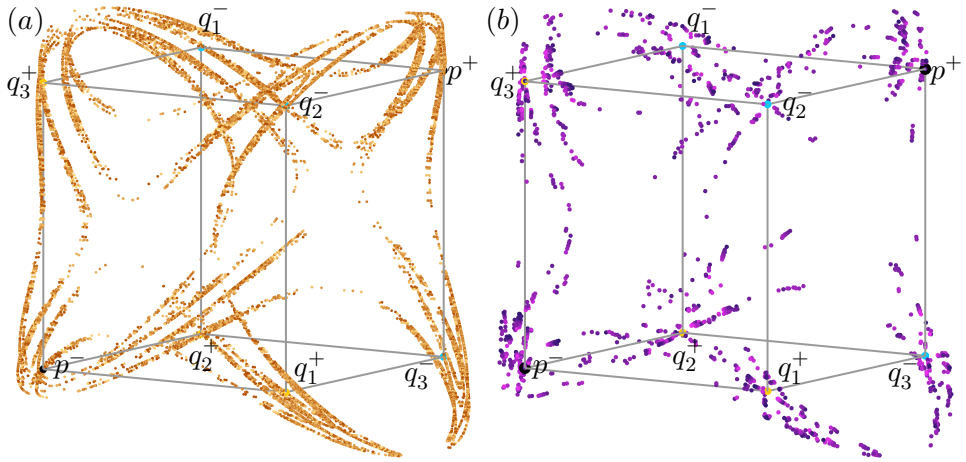


Figure 11: Representations of the chaotic, non-wandering set of $T$, shown in $\mathbb{R}^3$ with the cube with corners $p^+$, $p^-$, $q^+$ and $q^-$. Panel (a) shows 3,388 computed homoclinic orbits to $p^+$ with 28 points each (orange dots) for $k = \sqrt{20}$; and panel (b) shows 150 non-transverse heterodimensional connecting orbits with $k \in [4, 5]$ (purple dots) in a color gradient from darker for $k = 4$ to lighter for $k = 5$.

### 4.5 Investigating the chaotic set of $T$

The ability to find transverse homoclinic and non-transverse heterodimensional connecting orbits in a systematic and efficient way, via the construction of suitable pseudo-orbits as seeds for Newton's method, is a powerful tool for the study of complicated chaotic sets. Figure 11 shows two different approximations of the chaotic, non-wandering set of $T$, together with the cube formed by the corner points at $p^+$, $p^-$, and the period-three orbits $q^+$ and $q^-$.

Figure 11(a) shows $3,388$ different computed transverse homoclinic orbits to $p^+$ for the fixed parameter $k = \sqrt{20}$; each (approximate) homoclinic orbit comprises 28 points, and there are $94,864$ points in total. The homoclinic orbits were found by computing $W^u(p^+)$ up to $L = 21,140.95$ with the method from Section 2, and then constructing pseudo-orbits as explained in Section 4.1 for all local minima of $d(L)$ with $d(L) < 0.01$ that are associated with mesh points in the last fundamental domain. We then applied Newton's method to the BVP (9)–(11), starting from each of the $3,388$ seeds. In a post-processing step, we confirmed the validity of each computed homoclinic orbit by ensuring that their end points all lie within 0.05 of $p^+$. The homoclinic points in Fig. 11(a) are seen to accumulate on a complicated, seemingly connected set of curves.

Figure 11(b) shows a total of 150 different non-transverse heterodimensional connecting orbits from $p^+$ to $p^-$ with values of the parameter $k$ in the interval $[4, 5]$. They were found in the same manner as explained in Section 4.4, by constructing heterodimensional pseudo-orbits as seeds for the BVP (13)–(15). More precisely, we compared the computed intersection set $W^s(p^-) \cap \Sigma$, consisting of $29,995$ points, with the intersection set $W^u(p^+) \cap \Sigma$ restricted to a particular fundamental domain of $W^u(p^+)$. We then identified the closest 150 pairs of points, one from each set, and constructed the corresponding non-transverse heterodimensional pseudo-orbits. While determining these pairs, we found that some points in the fundamental domain of $W^u(p^+)$ are sufficiently close to more than one point in

$W^s(p^-) \cap \Sigma$; note that such pairs still yield topologically different non-transverse heterodimensional pseudo-orbits. Starting from these constructed seeds, Newton's method for the BVP (13)–(15) converged to the 150 non-transverse heterodimensional connecting orbits shown in Fig. 11(b). In comparison with the example in Figure 9, the pairs of points in $\Sigma$ lie closer to each other. As a result, the $k$-values for which these codimension-one objects exist, lie much closer to $k = \sqrt{20}$, namely, $k \in [4, 5]$ for all 150 solutions of the BVP. While the heteroclinic orbits in Figure 11(b) do not exist for the same $k$-value, they nevertheless, give us an impression of where the overall set of non-transverse heterodimensional orbits is located in phase space. In particular, notice that this set of points has a very similar shape to that of the transverse homoclinic orbits in panel (a). Our ongoing numerical investigations strongly suggest that the non-wandering set of $T$ and, hence, $T$ itself are robustly non-hyperbolic. In particular, this means that heterodimensional cycles occur robustly, and Figure 11 provides numerical evidence for this assertion.

# 5 Conclusions

We modified the algorithm from [5] for the computation of a one-dimensional (un)stable manifold of a fixed or periodic point of a diffeomorphism, so that it stores, effectively at no additional cost, approximate preimages for any point in the resulting mesh. This allows us to construct, or rather read off, pseudo-orbits of selected mesh points. The constructed pseudo-orbits serve as initial data or seeds for the solution of a boundary value problem that represents orbits of interest, including homoclinic and heteroclinic connecting orbits. Provided the mesh size of the computed mesh is sufficiently small, Newton's method will converge when starting from the respective pseudo-orbit, even if $\varepsilon$ is relatively large. The modified algorithm is available at `github.com/dcjulio`. It can be used to construct pseudo-orbits along any one-dimensional stable or unstable manifold of a diffeomorphism of interest.

We demonstrated the benefits of this modification with two examples. First, we showed how (a large number of) intersection points of the one-dimensional unstable manifold of a fixed point of a three-dimensional Hénon-like map with a chosen section can be found. These were then continued as curves in a parameter to determine whether or not there exists a blender, specifically, by checking the characterising property that a suitable projection of the intersection points is dense. As a second example we considered a one-parameter family of three-dimensional diffeomorphisms that exhibits a non-wandering set with partially hyperbolic dynamics. Here, we used pseudo-orbits to generate seeds for the systematic computation of thousands of transverse homoclinic orbits at a fixed value of the parameter, as well as of many non-transverse heterodimensional connecting orbits at corresponding specific parameter values.

The two examples we presented showcase the capability of our algortihm with the aim of motivating computations of connecting orbits more widely—as an efficient tool for investigating complicated dynamics in explicitly given parameter-dependent diffeomorphisms. Further research, including for the two families of diffeomorphism considered here, is ongoing and will be reported elsewhere.

## Acknowledgments

We thank Andy Hammerlindl for helpful discussions and for providing the BSc Honours thesis of his student Hua Chen Li. This work was supported by Royal Society Te Apārangi Marsden Fund grant #22-UOA-204.

## References

[1] Beyn, W.J., Kleinkauf, J.M.: The numerical computation of homoclinic orbits for maps. SIAM Journal on Numerical Analysis 34(3), 1207–1236 (1997)

[2] Bonatti, C., Crovisier, S., Díaz, L.J., Wilkinson, A.: What is ... a blender? Notices of the American Mathematical Society 63(10), 1175–1178 (2016)

[3] Bonatti, C., Díaz, L.J., Viana, M.: Dynamics Beyond Uniform Hyperbolicity. Encyclopaedia of Mathematical Sciences (EMS, vol. 102). Springer Berlin, Heidelberg (2005)

[4] Bowen, R.E.: Equilibrium States and the Ergodic Theory of Anosov Diffeomorphisms. $2^{rmnd}$ edition. Lecture Notes in Mathematics (LNM,volume 470). Springer Berlin, Heidelberg (2008)

[5] C'Julio, D., Krauskopf, B., Osinga, H.M.: Computing parametrised large intersection sets of 1D invariant manifolds: A tool for blender detection. Numerical Algorithms 96(3), 1079–1108 (2024)

[6] C'Julio, D., Krauskopf, B., Osinga, H.M.: Mind the gaps: emergence of blenders in a three-dimensional Hénon-like map with different orientation properties. Preprint, University of Auckland (2025)

[7] Díaz, L.J.: Robust nonhyperbolic dynamics and heterodimensional cycles. Ergodic Theory and Dynamical Systems 15(2), 291–315 (1995)

[8] Hénon, M.: A two-dimensional mapping with a strange attractor. Communications in Mathematical Physics 50(1), 69–77 (1976)

[9] Hittmeyer, S., Krauskopf, B., Osinga, H.M.: Interacting global invariant sets in a planar map model of wild chaos. SIAM Journal on Applied Dynamical Systems 12(3), 1280–1329 (2013)

[10] Hittmeyer, S., Krauskopf, B., Osinga, H.M., Shinohara, K.: Existence of blenders in a Hénon-like family: Geometric insights from invariant manifold computations. Nonlinearity 31(10), 239–267 (2018)

[11] Hittmeyer, S., Krauskopf, B., Osinga, H.M., Shinohara, K.: How to identify a hyperbolic set as a blender. Discrete and Continuous Dynamical Systems 40(12), 6815–6836 (2020)

[12] Hobson, D.: An efficient method for computing invariant manifolds of planar maps. Journal of Computational Physics 104(1), 14–22 (1993)

[13] Guckenheimer, J., Holmes, P.: Nonlinear Oscillations, Dynamical Systems, and Bifurcations of Vector Fields. Applied Mathematical Sciences (AMS, vol. 42). Springer New York (1983)

[14] Katok, A., Hasselblatt, B.: Introduction to the Modern Theory of Dynamical Systems. Cambridge University Press (1995)

[15] Keller, H.B.: Lectures on Numerical Methods in Bifurcation Problems. Tata Institute of Fundamental Research. Lectures on Mathematics and Physics (LMP, vol. 79). Springer New York (1987)

[16] Krauskopf, B., Osinga, H.M., Galán-Vioque, J.: Numerical Continuation Methods for Dynamical Systems: Path following and boundary value problems. Springer, Dordrecht (2007)

[17] Krauskopf, B., Osinga, H.M.: Globalizing two-dimensional unstable manifolds of maps. International Journal of Bifurcation and Chaos 8(3), 483–503 (1998)

[18] Krauskopf, B., Osinga, H.M.: Growing 1D and quasi-2D unstable manifolds of maps. Journal of Computational Physics 146(1), 404–419 (1998)

[19] Krauskopf, B., Rieß, T.: A Lin's method approach to finding and continuing heteroclinic connections involving periodic orbits. Nonlinearity 21(8), 1655–1690 (2008)

[20] Li, D., Turaev, D.: Persistence of heterodimensional cycles. Inventiones Mathematicae 236(3), 1413–1504 (2024)

[21] Li, H.C.: Numerically computing the stable and unstable manifolds of a three-dimensional map inspired by the Hénon map. BSc Honours thesis, Monash University, Melbourne (2021)

[22] Lomelí, H.E., Meiss, J.D.: Quadratic volume-preserving maps. Nonlinearity 11(3), 557–574 (1998)

[23] Palis, J., De Melo, W.: Geometric Theory of Dynamical Systems. Springer New York (1982)

[24] Palis, J., Takens, F.: Hyperbolicity and Sensitive Chaotic Dynamics at Homoclinic Bifurcations. Cambridge University Press (1993)

[25] Palmer, K.J.: Exponential dichotomies, the shadowing lemma and transversal homoclinic points. In: Kirchgraber, U., Walther, H.O. (eds) Dynamics Reported (Dynamics Reported, vol. 1). pp. 265–306. Vieweg+Teubner Verlag Wiesbaden (1988)

[26] Parker, T.S., Chua, L.O.: Practical Numerical Algorithms for Chaotic Systems. Springer New York (1989)

[27] Robinson, C.: Dynamical Systems: Stability, Symbolic Dynamics, and Chaos. $2^{rmnd}$ edition. CRC Press, Boca Raton (1998)

[28] Veltz, R.: BifurcationKit.jl. A Julia package to perform bifurcation analysis. Inria Sophia-Antipolis `hal.archives-ouvertes.fr/hal-02902346` (2020; last accessed January 2026)